Volume 11 | Number 22 | 14 June 2019 | Pages 10559–11034

Nanoscale

rsc.li/nanoscale

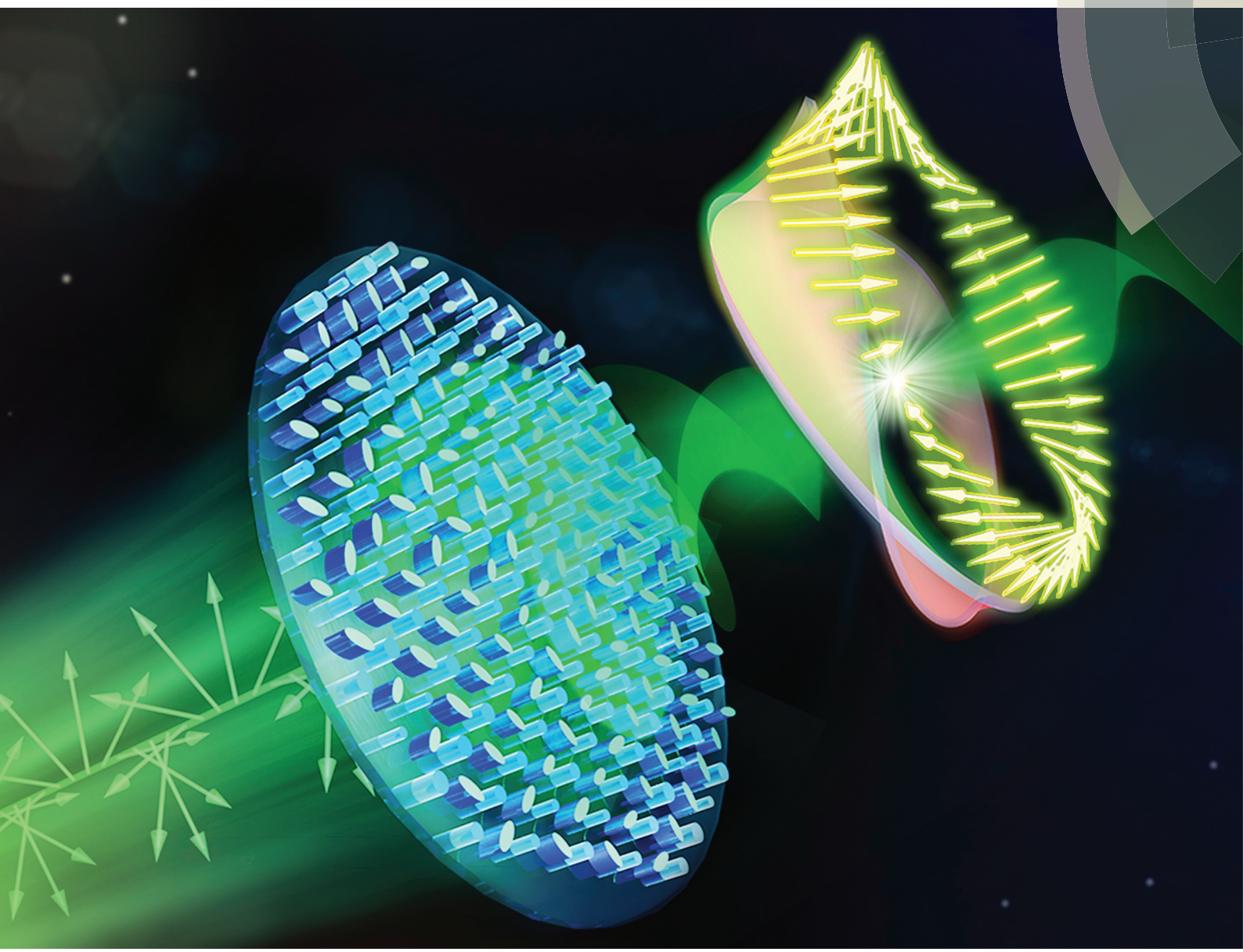

ISSN 2040-3372

ROYAL SOCIETY OF CHEMISTRY | Celebrating IYPT 2019

PAPER
Ting Xu *et al.*
Photonic spin-controlled generation and transformation of 3D optical polarization topologies enabled by all-dielectric metasurfaces

NCNST

Nanoscale

PAPER

View Article Online
View Journal | View Issue

Cite this: *Nanoscale*, 2019, **11**, 10646

Photonic spin-controlled generation and transformation of 3D optical polarization topologies enabled by all-dielectric metasurfaces

Pengcheng Huo,[a] Si Zhang,[a] Qingbin Fan,[a] Yanqing Lu[a,b] and Ting Xu *[a,b]

Received 4th December 2018,
Accepted 14th May 2019

DOI: 10.1039/c8nr09697j

rsc.li/nanoscale

Optical polarization topology is a spatially varying polarization structure, which usually exists around the polarization singularity. In three-dimensional (3D) space, optical polarization topologies mainly contain two fundamental structures, Möbius strip and twisted ribbon, depending on the parity of half-twist number. These spectacular topologies have been widely found in the existence of electric fields from multi-beam interference. Here, we propose and numerically demonstrate that, depending on the photonic spin state of light, an ultrathin all-dielectric metasurface can achieve efficient generation and transformation of two arbitrary 3D polarization topologies. The spin-controlled, tightly-focused Poincaré beams generated by the metasurface exhibit topologically stable 3D polarization topologies around the waist of the focal point. The preparation of such optical polarization topologies may have potential applications in compact complex beam engineering, optical signal multiplexing and optical fabrication of microstructures with nontrivial topology.

Introduction

Polarization, as one of the most fundamental properties of light, plays an important role in many optical applications, such as high-resolution imaging,[1,2] optical tweezers,[3,4] and multi-dimensional optical data storage.[5] In recent years, with the development of topology in nanophotonics,[6–8] optical polarization topology has attracted much attention due to its potential for complex structured beam engineering. Originating from the vectorial features of multi-beam interference, many interesting polarization topologies, such as *lemon*, *star* and *monstar*, have been used to describe the vectorial patterns in the transverse plane of a paraxial optical field.[9] These two-dimensional (2D) polarization topologies are formed by a rotation arrangement of the major and minor axes of the surrounding polarization ellipses following a closed circular path centered on a phase singular point. When the major and minor axes of the surrounding polarization ellipses are generally tilted out of the transverse plane, three-dimensional (3D) polarization topologies on the closed circular paths will be generated.

The spectacular 3D polarization topologies have many fundamental forms, mainly including Möbius strip and twisted ribbon,[10] which are determined by the parity of their half-twist numbers. The polarization Möbius strips are 3D geometrical structures with arbitrary odd numbers of half-twist, fascinating for their peculiar property of being non-orientable surfaces with only one-side and one-edge.[11] When the geometrical structures contain arbitrary even numbers of half-twist, losing the special single-side and single-edge topological properties, they become twisted ribbons. Based on the different twisting directions, both Möbius strips and twisted ribbons can form left-handed or right-handed helicity structures. Schematics of a right-handed helicity Möbius strip with one half-twist and a left-handed helicity twisted ribbon with two half-twists are respectively shown in Fig. 1a and b.

So far, there are several approaches to generate 3D polarization topologies.[12–16] For example, by using the non-collinear superposition of two unfocused paraxial circularly polarized beams of opposite handedness carrying different orbital angular momentums (OAMs), a nonparaxial 3D polarization topology can be generated at the beams' intersection plane.[12,16] Yet another, by employing commercial liquid crystal *q*-plate and objective lens with high numerical aperture, one can obtain 3D polarization structures appearing around the waist of the focal point.[13] These implementations of 3D polarization topologies have greatly promoted the understanding to the basic electromagnetic theory. However, above generation

[a]*National Laboratory of Solid State Microstructures, College of Engineering and Applied Sciences and Collaborative Innovation Centre of Advanced Microstructures, Nanjing University, Nanjing 210093, China. E-mail: xuting@nju.edu.cn*
[b]*Key Laboratory of Intelligent Optical Sensing and Manipulation, Ministry of Education, Nanjing University, Nanjing 210093, China*

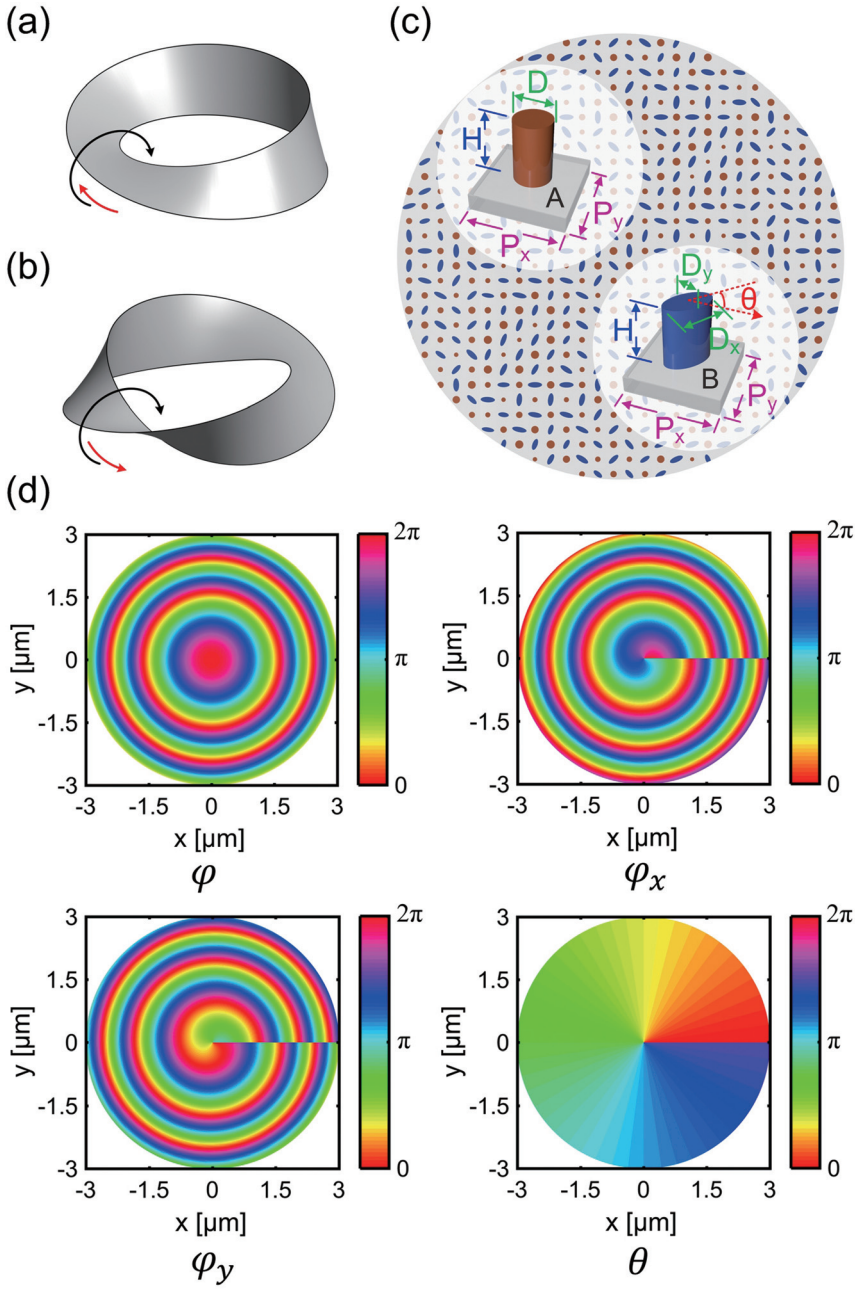

Fig. 1 Schematic diagrams of (a) a right-handed helicity Möbius strip with one half-twist and (b) a left-handed helicity twisted ribbon with two half-twists. (c) Schematic diagram of the designed all-dielectric metasurface element. Top-left inset is the cylindrical nanopost with a given height H and an adjustable diameter D. Bottom-right inset is the elliptical nanopost with a fixed height H and a varying long axis D_x and short axis D_y. Each elliptical nanopost has an orientation angle θ. The cylindrical and elliptical nanoposts are arranged in a square lattice on the SiO_2 substrate. (d) Calculated phase shifts φ, φ_x and φ_y and rotation angle θ of the designed metasurface for $m = 1$, $n = -2$, $\lambda = 532$ nm and $f = 2250$ nm.

approaches always rely on bulky optical setups with fairly large footprints and long working distance, which are difficult to be integrated into a compact nanophotonic platform. In order to realize the miniaturization of the structure, a small and simple optical system consisting of high refractive index spherical resonators is proposed to generate polarization Möbius strips.[15] Nevertheless, how to use photonic spin states to control and multiplex the topological transformation of generated 3D polarization structures is still a major scientific and technological issues. These abilities could further increase the degree of freedom to manipulate light and are highly desired in real applications.

In this paper, we propose and numerically demonstrate the design of a single-layer, ultrathin metasurface incorporating subwavelength phase shift structures that is able to circumvent above limitations and realize efficient generation and trans-

formation of arbitrary 3D polarization topologies. We stress that, by switching the photonic spin state of incident light, controlled topological transformation can be realized between two forms of 3D polarization topologies (Möbius strip and twisted ribbon) with arbitrary half-twist number, which is unachievable for the conventional approaches.

Results and discussion

A Poincaré beam,[17] whose polarization in the transverse plane (x–y plane) spans the entire surface of the Poincaré sphere, can be obtained by coaxially superimposing a pair of circularly polarized Gaussian beam and spiral-phase Laguerre–Gauss (LG) beam with opposite handedness:

$$\mathbf{E}(\mathbf{r}) = \cos\left(\frac{\delta}{2}\right)G(\mathbf{r})\mathbf{e_1} + \sin\left(\frac{\delta}{2}\right)e^{i\chi}\mathrm{LG}_{p,l}(\mathbf{r})\mathbf{e_2} \quad (1)$$

where $\mathbf{e_1}$ and $\mathbf{e_2}$ are unit vectors of two orthogonal circular polarizations; δ and χ respectively are amplitude coefficients and relative phase between two orthogonal polarization states; $G(\mathbf{r})$ is the Gaussian beam; $\mathrm{LG}_{p,l}(\mathbf{r})$ is the LG beam with radial index p and azimuthal index l.[18] The index l regulates azimuthal angular momentum of the LG beam and is related to the topological charge. When a Poincaré beam is tightly focused, a strong longitudinal component along the beam axis (z-direction) is generated and the paraxial approximation breaks down. As a result, the polarization ellipses of the beam are tilted out of the transverse plane and 3D polarization topologies, which are flattened and therefore unobservable in the paraxial case, now become visible.

Assume the incident light upon the planar optical element are in two orthogonal spin states $|L\rangle = \frac{1}{\sqrt{2}}\begin{bmatrix}1\\ i\end{bmatrix}$ and $|R\rangle = \frac{1}{\sqrt{2}}\begin{bmatrix}1\\ -i\end{bmatrix}$, where $|L\rangle$ and $|R\rangle$ denote left- and right-circular polarization (LCP and RCP) in the linear polarization basis. Based on the eqn (1), in order to independently generate two different Poincaré beams for the incident Gaussian beam propagating along the z-direction respectively in LCP and RCP states, the optical element should perform the beam transformation

$$\mathrm{LCP}: |L\rangle \rightarrow \cos\left(\frac{\delta}{2}\right)|L\rangle + \sin\left(\frac{\delta}{2}\right)e^{i\chi}e^{im\phi}|R\rangle \quad (2)$$

$$\mathrm{RCP}: |R\rangle \rightarrow \cos\left(\frac{\delta}{2}\right)|R\rangle + \sin\left(\frac{\delta}{2}\right)e^{i\chi}e^{in\phi}|L\rangle \quad (3)$$

where the first term is the spin-maintained states that has the same handedness as the input beam, while the second one is the spin-flipped states that has opposite handedness and the transmitted beam has acquired an azimuthally dependent phase factor $e^{im\varphi}(e^{in\varphi})$, which indicates the beam has carried $m\hbar$ ($n\hbar$) OAM. Here m (n) is any integer and φ is the azimuthal angle. Consequently, the optical device can be described by a Jones matrix J which acts independently on the two orthogonal input states and takes the form as

$$J = \begin{bmatrix} \cos\left(\frac{\delta}{2}\right) + \frac{1}{2}\sin\left(\frac{\delta}{2}\right)e^{i\chi}(e^{im\phi} + e^{in\phi}) & \frac{i}{2}\sin\left(\frac{\delta}{2}\right)e^{i\chi}(e^{im\phi} - e^{in\phi}) \\ \frac{i}{2}\sin\left(\frac{\delta}{2}\right)e^{i\chi}(e^{im\phi} - e^{in\phi}) & \cos\left(\frac{\delta}{2}\right) - \frac{1}{2}\sin\left(\frac{\delta}{2}\right)e^{i\chi}(e^{im\phi} + e^{in\phi}) \end{bmatrix} \quad (4)$$

Since this matrix is symmetric, it can be decomposed into the following form $J = P\Delta P^{-1}$, where P is a real unitary matrix whose columns are the eigenvectors of J, and Δ is a diagonal matrix whose elements are the eigenvalues of J. By solving the characteristic equation of the Jones matrix J, we can find its eigenvalues and eigenvectors, and then J can be decomposed into the following form,

$$J(\phi) = \cos\left(\frac{\delta}{2}\right)I + \sin\left(\frac{\delta}{2}\right)e^{i\chi}P(\phi)\begin{bmatrix} e^{\frac{i}{2}(m+n)\phi} & 0 \\ 0 & e^{\frac{i}{2}(m+n)\phi - i\pi} \end{bmatrix}P^{-1}(\phi) \quad (5)$$

where I is unit matrix.

To create 3D polarization topologies efficiently, the generated Poincaré beam need to be tightly focused. Therefore, we can add an additional polarization-independent focusing phase φ_f to the planar optical element that makes the output Poincaré beam to focus along the beam axis. As a result, the Jones matrix J should perform the following transformation,

$$J(\varphi)e^{i\varphi_f(r,\varphi)} \rightarrow J(r,\varphi) \quad (6)$$

$$\varphi_f(r,\phi) = \frac{2\pi}{\lambda}\left(f - \sqrt{r^2 + f^2}\right) \quad (7)$$

where λ is the operation wavelength, r and φ are the radius and azimuthal angle of each point of the device in the polar coordinates, f is the focal length. According to expressions (5)–(7), now we can derive the final form of the Jones matrix that guarantees the photonic spin-controlled generation of 3D polarization topologies, as

$$J(r,\phi) = \cos\left(\frac{\delta}{2}\right)e^{i\varphi_f(r,\phi)}I + \sin\left(\frac{\delta}{2}\right)e^{i\chi}P(\phi) \times \begin{bmatrix} e^{\frac{i}{2}(m+n)\phi + i\varphi_f(r,\phi)} & 0 \\ 0 & e^{\frac{i}{2}(m+n)\phi - i\pi + i\varphi_f(r,\phi)} \end{bmatrix}P^{-1}(\phi) \quad (8)$$

The right side of this expression contains two terms, in which the matrix structure is different. The unit matrix I of the first term requires that the optical element should be isotropic. Combining the exponential term, it can implement a phase shift $\varphi_f(r,\varphi)$ for incident light with arbitrary handedness. The diagonal matrix of the second term requires that the optical element should have birefringent response, and the diagonal

elements respectively determine the phase shifts along fast and slow axes. The matrix $P(\phi)$ is a rotation matrix that determines the orientation angle of birefringent fast axis relative to the reference coordinate. Therefore, it is imperative to find a set of nanostructures with proper phase shifts and orientation angles covering an entire 2π phase range.

Fig. 1c shows the schematic diagram of the proposed planar metasurface element. As an exciting platform for flat optics, metasurface recently have attracted a lot of attention and made great progress in nanophotonics devices.[19–36] As shown in Fig. 1c, the designed metasurface contains two sets of nanostructures, *isotropic* nanopost A and *anisotropic* nanopost B, arranged periodically in a square lattice. All the nanostructures are made of titanium dioxide (TiO_2), a high-index transparent dielectric widely used at visible frequency. The nanopost A is a cylindrical TiO_2 pillar with a fixed height H and a varying diameter D, which can be used for controlling polarization independent phase shift $\varphi(r,\phi)$. The nanopost B is an elliptical TiO_2 pillar with a fixed height H and a varying long axis D_x and short axis D_y. Each of these elliptical structures is actually a wave plate, where the propagation phase shifts $\varphi_x(r,\phi)$ and $\varphi_y(r,\phi)$ along the two axes are controlled by varying long axis D_x and short axis D_y, and the geometric phase are controlled by the orientation angle θ of fast axis. Based on the arrangement of these structures, two sets of independent phase profiles can be imparted on incident light in LCP and RCP states.

According to the expression (8), for any value of m, n, λ and f, we can obtain the analytical expression of the required phase shifts and orientation angles for two sets of nanopost as follows,

Nanopost A:

$$\varphi(r,\phi) = \frac{2\pi}{\lambda}\left(f - \sqrt{r^2+f^2}\right) \tag{9}$$

Nanopost B:

$$\varphi_x(r,\phi) = \frac{1}{2}(m+n)\phi + \frac{2\pi}{\lambda}\left(f - \sqrt{r^2+f^2}\right) \tag{10}$$

$$\varphi_y(r,\phi) = \frac{1}{2}(m+n)\phi - \pi + \frac{2\pi}{\lambda}\left(f - \sqrt{r^2+f^2}\right) \tag{11}$$

$$\theta(r,\phi) = \frac{1}{4}(m-n)\phi \tag{12}$$

To demonstrate the photonic spin-controlled generation and transformation of arbitrary 3D polarization topologies using metasurface, here we consider two polarization topologies, including a right-handed helicity Möbius strip with three half-twists (m = 1) and a left-handed helicity twisted ribbon with four half-twists (n = −2), respectively corresponding to LCP and RCP incident light at λ = 532 nm. The metasurface has a numerical aperture of 0.8 and the focal length f = 2250 nm. Based on the expressions (9)–(12), the required phase shifts and rotation angle of the metasurface are calculated and shown in Fig. 1d.

A broad range of TiO_2 nanoposts with a fixed height of 600 nm but varying diameters are calculated to find the proper structural parameters for the cylindrical and elliptical nanoposts. Fig. 2a–d show the transmission coefficients and phase shifts as a function of elliptical nanorod diameters at the wavelength of 532 nm. Each point in the spectra graphs corresponds to a nanorod with specific (D_x, D_y) combination. Two sets of eight-order cylindrical nanopost A and elliptical nanopost B with high transmission efficiencies are chosen to form the metasurface. These nanoposts are arranged in a square lattice with lattice constant $P_x = P_y$ = 480 nm, leading to two phase profiles with independent response to LCP and RCP light.

As shown in Fig. 3a, for the LCP light incident on the metasurface, Fig. 3b–d show the simulated intensity distributions of three individual electric field components (E_x, E_y and E_z) associated with phase distributions of the tightly-focused beam at the focal plane. The numerical simulation is implemented by using the commercial finite-difference time-domain (FDTD) software (Lumerical Solutions). The intensity and phase distribution of three individual electric field components are obtained by setting a monitor at the focal plane. Perfectly matched layer conditions are used along x, y, and z direction. The grid size along the x, y, and z direction is 1 nm × 1 nm × 1 nm, respectively. As plotted in Fig. 3b and c, both E_x and E_y have an asymmetric intensity pattern and show a vortex phase distribution, which originates from the interference between their spin-maintained states without OAM and spin-flipped states carrying $m\hbar$ OAM (m = 1). In terms of E_z, because of the spin-to-orbital conversion under the condition of tightly focusing, the spin-maintained state obtains an additional $-\hbar$ OAM while the spin-flipped state obtains an additional $+\hbar$ OAM.[37] As a result, E_z at the focal plane shows a composite-vortex pattern generated by the interference between two spin states respectively carrying $-\hbar$ and $2\hbar$ OAM (Fig. 3d). Combing E_x, E_y and E_z, inset of Fig. 3e shows the intensity distribution of total electric field E at the focal plane, which has a threefold symmetry pattern. This results from the nonparaxiality of focusing Poincaré beam and predicts the half-twist number of polarization structure. In addition, the efficiency of generation of optical states is estimated by measuring the metasurface's focusing efficiency of incident light, which is about 18% in the simulation. This efficiency is partly limited by the large numerical aperture (0.8) of the designed metasurface element and can be further improved by optimizing the structural parameters.

In principle, 3D orientation of the polarization ellipse around the optical axis of the focal plane can be traced by solving Berry formulas introduced in ref. 38. Here, based on the Berry formulas and the simulated electric fields at the focal plane, we calculate the major axis of the 3D-polarization ellipse of the all points lying on a circle centered at the beam axis. For LCP incident light, Fig. 3e shows the retrieved polarization topology of the tightly focused Poincaré beam generated by metasurface, which describes a three half-twists Möbius strip. The twisting direction of polarization Möbius strip is

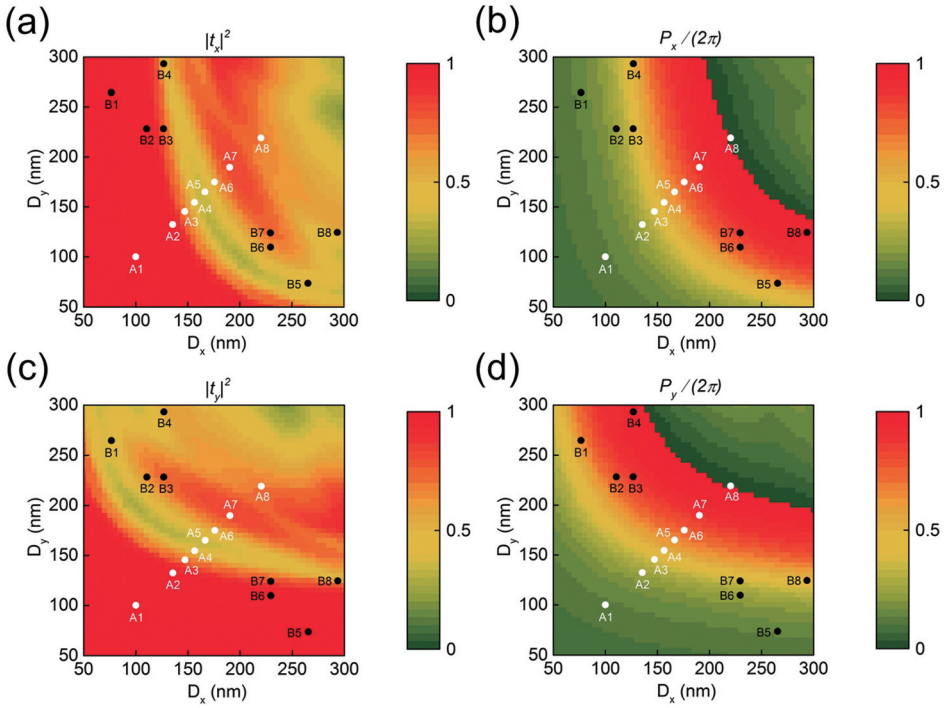

Fig. 2 (a) Transmission coefficient $|t_x|^2$ and (b) phase shift P_x of x-polarized light for the elliptical TiO_2 nanorods. (c) The Transmission coefficient $|t_y|^2$ and (d) phase shift P_y can be obtained by switching the x- and y-axes. Two sets of eight-order discrete structures A and B used in the metasurface design have been shown in the graph. The polarization conversion efficiencies of the eight fundamental structures in the set of Nanopost B are 96%(B1, B5), 95%(B2, B6), 96%(B3, B7) and 84%(B4, B8), respectively.

right-handed, opposite to the helicity of the input beam. In order to enhance the visualization of the 3D orientation of the polarization topology, one half of the major axis of the polarization ellipse is colored blue and the other half is colored green. It can be clearly seen that an opening flip appears in the strip where two polarization vectors parallel to each other but with opposite directions. This indicates there is a phase different of π in the electric field with the evolution of major axis of the polarization ellipses following one circular path. As a result, a point on the polarization strip edge can return to its origin after moving through all the edge path, which is well suited to the single-edge and single-side characters of Möbius strip.

On the other side, when the incident light is switched from LCP ($m = 1$) to RCP ($n = -2$), as shown in Fig. 3f, the corresponding simulated intensity distributions of E_x, E_y and E_z associated with phase distributions of the tightly-focused beam at the focal plane for are given in Fig. 3g–i, which result from the interference between spin-maintained and spin-flipped states respectively with OAM of 0 and $-2\hbar$ for E_x and E_y, and $\hbar$ and $-3\hbar$ for E_z. Inset of Fig. 3j shows intensity distribution of the total electric field E at the focal plane. In contrast to the threefold symmetry pattern for LCP light, here E has a fourfold symmetry pattern. Based on the Berry formulas, we calculate and retrieve the polarization topology of the tightly focused Poincaré beam generated by metasurface for RCP light, which describes a left-handed helicity twisted ribbon with four half-twists (Fig. 3j). Different from the Möbius strip, the directions of polarization vectors smoothly change along the circular path and there is no opening flip in the twisted ribbon. Consequently, a point on the edge can never return to its origin by moving through all the edge path and thus the twisted ribbon has two individual edges and sides.

Above 3D polarization topologies are reconstructed at the focal plane $z = 0$ with focal radius of 150 nm. Fig. 4 gives the reconstructed polarization topologies in the transverse planes perpendicular to the optical axis and located at $z = -\lambda/4$ and $z = \lambda/4$. The Möbius strips (Fig. 4a and b) and twisted ribbons (Fig. 4c and d) still can be generated by the metasurface respectively from LCP and RCP incident light. The only difference between these two Möbius strips (twisted ribbons) is that their polarization vectors are in opposite directions (green and blue edges are flipped), which is mainly resulted from the phase difference after a propagation distance of $\lambda/2$. Except this, their polarization topologies remain similar. In addition, Fig. 5 shows the reconstructed optical polarization topologies with different radii surrounding the center point of the focal plane. It can be clearly seen that when the radius of the focal spot ranges from 100 nm to 200 nm, all the reconstructed 3D polarization topologies still keep the structures of Möbius strips with three half-twists for LCP light (Fig. 5b–d) and twisted ribbons with four half-twists for RCP light (Fig. 5f–h), respectively. These results verify the topologically stable existence of 3D polarization topologies around the focal volume.

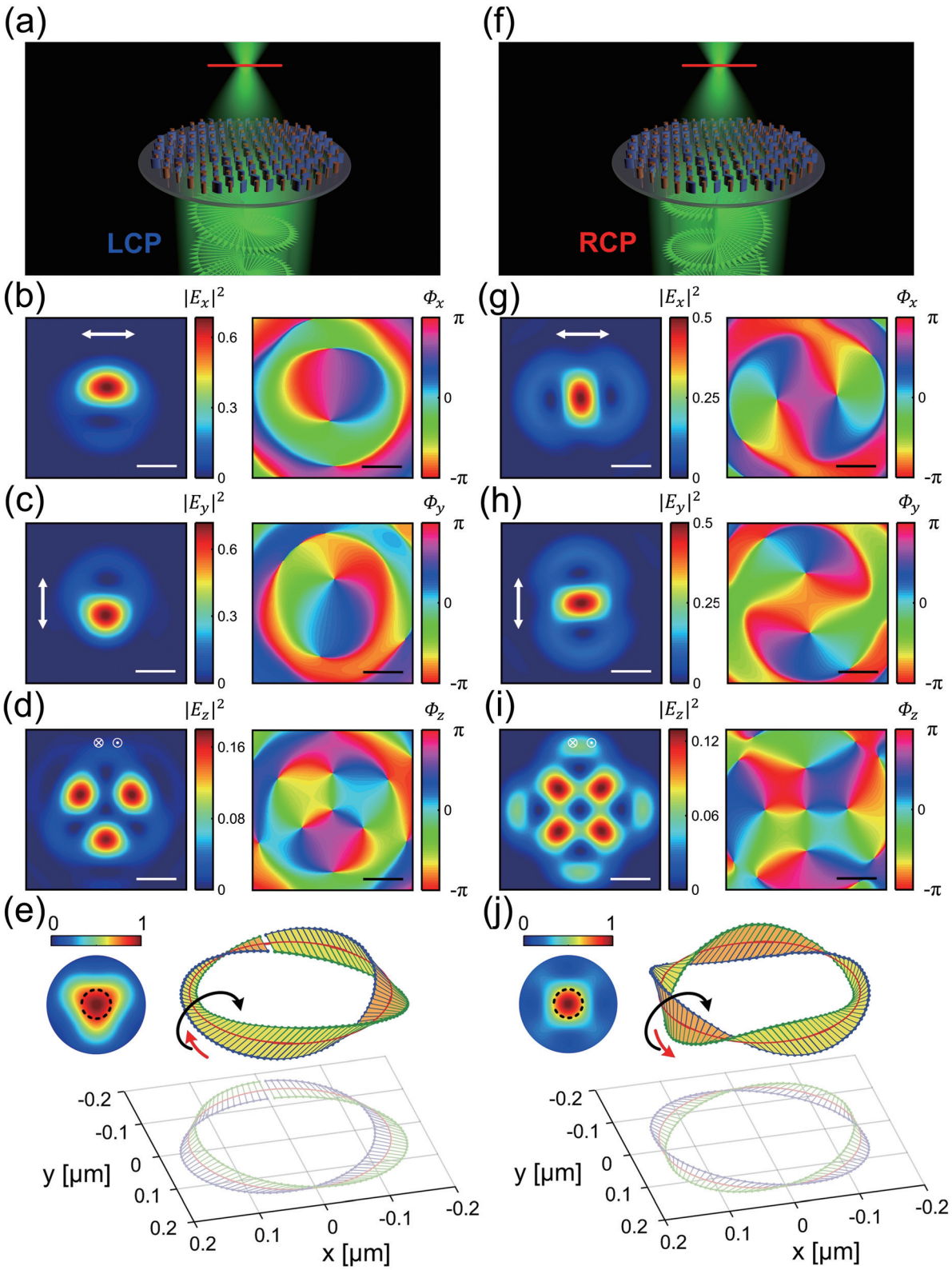

Fig. 3 The schematic diagrams and simulation results for LCP (a–e) and RCP (f–j) light incident on the metasurface and forming 3D polarization topologies. The simulated electric field intensities and phase distributions of E_x, E_y, and E_z of the tightly-focused Poincaré beam at the focal plane for (b–d) LCP and (g–i) RCP incident light. Scale bar, 400 nm. The retrieved polarization topologies at the focal plane, which describe (e) a right-handed helicity Möbius strip with three half-twists and (j) a left-handed helicity twisted ribbon with four half-twists. Here the topological structures are traced with the major axis of the 3D-polarization ellipse as a function of position on a circle of 150 nm radius, shown as the dash black line in the top-left inset of intensity distribution of E. The projections of polarization major axis onto x–y plane clearly indicate the half-twist number of the generated structures.

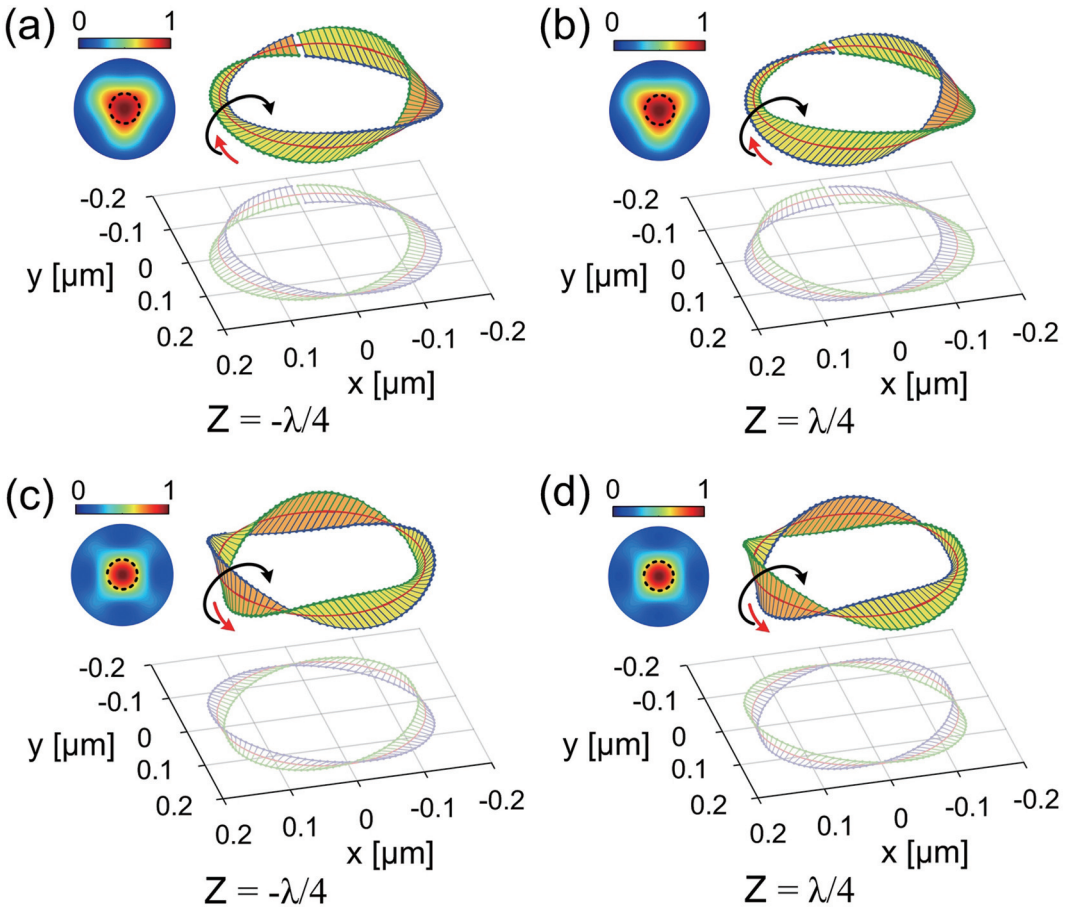

Fig. 4 For the LCP incident light, (a) and (b) show retrieved polarization Möbius strips in the transverse planes located at $z = -\lambda/4$ and $z = \lambda/4$, respectively. For the RCP incident light, (c) and (d) show retrieved polarization twisted ribbons in the transverse planes located at $z = -\lambda/4$ and $z = \lambda/4$, respectively.

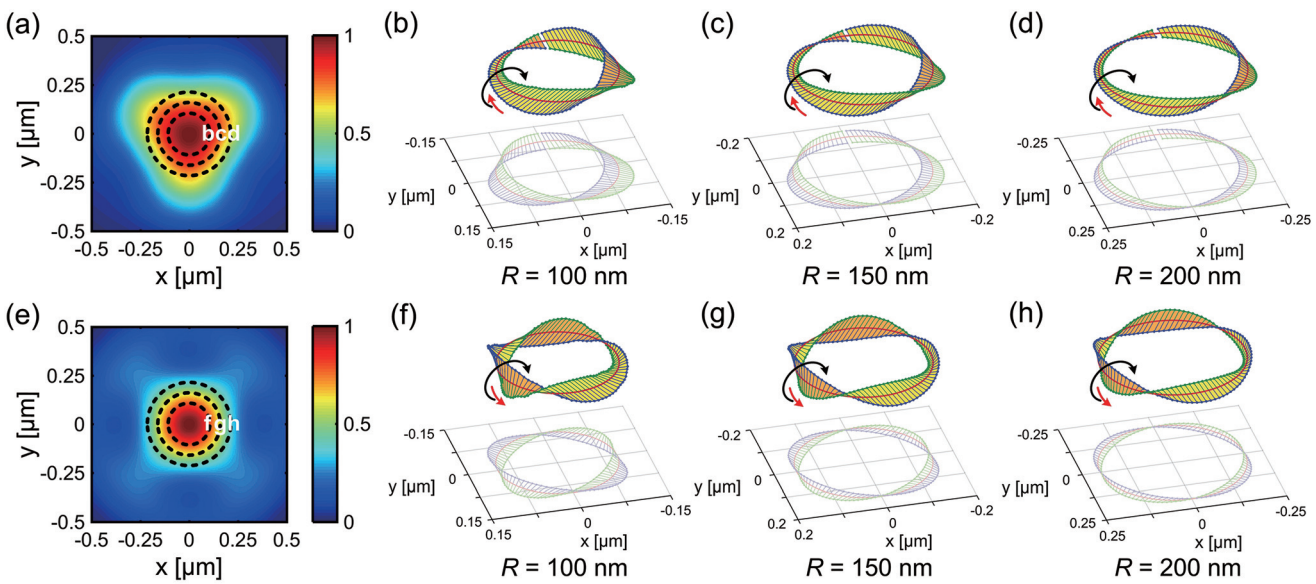

Fig. 5 (a) The total electric field intensity at the focal plane for LCP incident light ($m = 1$). (b), (c) and (d) are the retrieved three half-twists, right-handed helicity Möbius strip with different radii of 100 nm, 150 nm and 200 nm. (e) The total electric field intensity at the focal plane for RCP incident light ($n = -2$). (f), (g) and (h) are the retrieved four half-twists, left-handed helicity twisted ribbon with different radii of 100 nm, 150 nm and 200 nm. These results show that the optical 3D polarization structures are topologically stable with different radius.

Conclusion

In conclusion, we have proposed and numerically demonstrated that an ultrathin metasurface element formed by all-dielectric subwavelength nanopost nanostructures is able to achieve generation and transformation of two arbitrary 3D polarization topologies based on the polarization state of incident light. In real experiment, several approaches, such as using single nanoparticle,[16] and single molecule[39] as electric field probes, can be employed to precisely detect the electric field distributions and visualize the transformation of arbitrary 3D polarization topologies. We envision the preparation of such optical polarization topologies may have potential applications in 3D information storage encoded with polarization, compact complex beam engineering and optical signal multiplexing. In addition, these specific pattern also can be used to manipulate the nanoparticles composed of medium that strongly interact with polarization of light and optically fabricate the microstructures with nontrivial topology.

Conflicts of interest

There are no conflicts to declare.

Acknowledgements

The work is supported by the Key Research and Development Program from Ministry of Science and Technology of China (2017YFA0303700) and National Natural Science Foundation of China (61575092 and 11774163).

References

1 H. F. Wang, T. B. Huff, D. A. Zweifel, W. He, P. S. Low, A. Wei and J. X. Cheng, In vitro and in vivo two-photon luminescence imaging of single gold nanorods, *Proc. Natl. Acad. Sci. U. S. A.*, 2005, **102**, 15752.
2 M. P. Bacjlund, A. Arbabi, P. N. Petrov, E. Arbabi, S. Saurabh, A. Faraon and W. E. Moerner, Removing orientation-induced localization biases in single-molecule microscopy using a broadband metasurface mask, *Nat. Photonics*, 2016, **10**, 459.
3 M. Padgett and R. Bowman, Tweezers with a twist, *Nat. Photonics*, 2011, **5**, 343.
4 V. Shvedov, A. R. Davoyan, C. Hnatovsky, N. Engheta and W. Krolikowski, A long-range polarization-controlled optical tractor beam, *Nat. Photonics*, 2014, **8**, 846.
5 P. Zijlstra, J. W. M. Chon and M. Gu, Five-dimensional optical recording mediated by surface plasmons in gold nanorods, *Nature*, 2009, **459**, 410.
6 L. Lu, J. D. Joannopoulos and M. Soljacic, Topological photonics, *Nat. Photonics*, 2014, **8**, 821.
7 A. B. Khanikaev and G. Shvets, Two-dimensional topological photonics, *Nat. Photonics*, 2017, **11**, 763.
8 W. L. Gao, M. Lawrence, B. Yang, F. Liu, F. Z. Fang, B. Beri, J. Li and S. Zhang, Topological Photonic Phase in Chiral Hyperbolic Metamaterials, *Phys. Rev. Lett.*, 2015, **114**, 037402.
9 M. V. Berry and J. H. Hannay, Umbilic points on Gaussian random surfaces, *J. Phys. A: Math. Gen.*, 1977, **10**, 1809.
10 I. Freund, Cones, spirals, and Möbius strips, in elliptically polarized light, *Opt. Commun.*, 2005, **249**, 7.
11 C. A. Pickover, *The Möbius Strip: Dr. August Möbius's Marvelous Band in Mathematics, Games, Literature, Art, Technology, and Cosmology*, Thunder's Mouth Press, New York, 2005.
12 I. Freund, Multitwist optical Möbius strips, *Opt. Lett.*, 2010, **35**, 148.
13 T. Bauer, P. Banzer, E. Karimi, S. Orlov, A. Rubano, L. Marrucci, E. Santamato, R. W. Boyd and G. Leuchs, Observation of optical polarization Möbius strips, *Science*, 2015, **347**, 964.
14 T. Bauer, M. Neugebauer, G. Leuchs and P. Banzer, Optical Polarization Mobius Strips and Points of Purely Transverse Spin Density, *Phys. Rev. Lett.*, 2016, **117**, 013601.
15 A. Garcia-Etxarri, Optical Polarization Mobius Strips on All-Dielectric Optical Scatterers, *ACS Photonics*, 2017, **4**, 1159–1164.
16 E. J. Galvez, I. Dutta, K. Beach, J. J. Zeosky, A. A. Jones and B. Khajavi, Multitwist Möbius Strips and Twisted Ribbons in the Polarization of Paraxial Light beams, *Sci. Rep.*, 2017, **7**, 13653.
17 M. Beckley, T. G. Brown and M. A. Alonso, Full Poincaré beams, *Opt. Express*, 2010, **18**, 10777.
18 A. E. Siegman, *Lasers*, University Science Books, Herndon, VA, 1986.
19 Z. Bomzon, G. Binerer, V. Kleiner and E. Hasman, Space-variant Pancharatnam-Berry Phase Optical Elements with Computrt-generated Subwavelength Gratings, *Opt. Lett.*, 2002, **27**, 1141–1143.
20 N. Yu, P. Genevent, M. A. Kats, F. Aieta, J. Tetienne, F. Capasso and Z. Gaburro, Light propagation with phase discontinuities: Generalized laws of reflection and refraction, *Science*, 2011, **334**, 333.
21 X. Ni, N. K. Emani, A. V. Kildishev, A. Boltasseva and V. M. Shalaev, Broadband Light Bending with Plasmonic Nanoantennas, *Science*, 2012, **335**, 427.
22 E. Karimi, S. A. Schulz, I. D. Leon, H. Qassim, J. Upham and R. W. Boyd, Generating Optical Orbital Angular Momentum at Visible Wavelengths Using a Plasmonic Metasurface, *Light: Sci. Appl.*, 2014, **3**, e167.
23 J. Lee, M. Tymchenko, C. Argyropoulos, P. Chen, F. Lu, F. Demmerle, G. Boehm, M. Amann, A. Alu and M. A. Belkin, Giant nonlinear response from plasmonic metasurfaces coupled to intersubband transitions, *Nature*, 2014, **511**, 65.
24 X. Luo, Principles of electromagnetic waves in metasurfaces, *Sci. China: Phys., Mech. Astron.*, 2015, **58**, 594201.
25 M. Decker, I. Staude, M. Falkner, J. Dominguez, D. N. Neshev, I. Brener, T. Pertsch and Y. S. Kivshar, High-

efficiency dielectric Huygens' surfaces, *Adv. Opt. Mater.*, 2015, **3**, 813–820.

26 A. Arbabi, Y. Horie, M. Bagheri and A. Faraon, Dielectric metasurfaces for complete control of phase and polarization with subwavelength spatial resolution and high transmission, *Nat. Nanotechnol.*, 2015, **10**, 937.

27 G. X. Zheng, H. Muhlenbernd, M. Kenney, G. X. Li, T. Zentgraf and S. Zhang, Metasurface holograms reaching 80% efficiency, *Nat. Nanotechnol.*, 2015, **10**, 308.

28 D. Tang, C. Wang, Z. Zhao, Y. Wang, M. Pu, X. Li, P. Gao and X. Luo, Ultrabroadband superoscillatory lens composed by plasmonic metasurfaces for subdiffraction light focusing, *Laser Photonics Rev.*, 2015, **9**, 713–719.

29 M. Pu, X. Li, X. Ma, Y. Wang, Z. Zhao, C. Wang, C. Hu, P. Gao, C. Huang, H. Ren, X. Li, F. Qin, J. Yang, M. Gu, M. Hong and X. Luo, Catenary optics for achromatic generation of perfect optical angular momentum, *Sci. Adv.*, 2015, **1**, e1500396.

30 Z. Zhao, M. Pu, H. Gao, J. Jin, X. Li, X. Ma, Y. Wang, P. Gao and X. Luo, Multispectral optical metasurfaces enabled by achromatic phase transition, *Sci. Rep.*, 2015, **5**, 15781.

31 X. Li, M. Pu, Z. Zhao, X. Ma, J. Jin, Y. Wang, P. Gao and X. Luo, Catenary nanostructures as compact Bessel baem generators, *Sci. Rep.*, 2016, **6**, 20524.

32 E. Maguid, I. Yulevich, D. Veksler, V. Kleiner, M. L. Brongersma and E. Hasman, Photonic spin-controlled multifunctional shared-aperture antenna array, *Science*, 2016, **352**, 1202.

33 M. Khorasaninejad, W. T. Chen, R. C. Devlin, J. Oh, A. Y. Zhu and F. Capasso, Metalenses at visible wavelengths: Diffraction-limited focusing and subwavelength resolution imaging, *Science*, 2016, **352**, 1190.

34 Y. Ra'di, D. L. Sounas and A. Alu, Meta-Gratings: Beyond the Limits of Graded Metasurfaces for Wavefront Control, *Phys. Rev. Lett.*, 2017, **119**, 067404.

35 A. E. Minovich and A. V. Zayats, Geometric-Phase Metasurfaces Based on Anisotropic Reflection: Generalized Design Rules, *ACS Photonics*, 2018, **5**, 1755–1761.

36 G. Li, G. Sartorello, S. Chen, L. H. Nichollsm, K. F. Li, T. Zentgraf, S. Zhang and A. V. Zayats, Spin and Geometric Phase Control Four-Wave Mixing from Metasurfaces, *Laser Photonics Rev.*, 2018, **12**, 1800034.

37 Y. Zhao, J. S. Edgar, G. D. M. Jeffries, D. McGloin and D. T. Chiu, Spin-to-Orbital Angular Momentum Conversion in a Strongly Focused Optical Beam, *Phys. Rev. Lett.*, 2007, **99**, 073901.

38 M. V. Berry, Index formulae for singular lines of polarization, *J. Opt. A: Pure Appl. Opt.*, 2004, **6**, 675.

39 L. Novotny, M. R. Beversluis, K. S. Youngworth and T. G. Brown, Longitudinal field modes probed single molecules, *Phys. Rev. Lett.*, 2001, **86**, 5251.

